ISSN 0361-7688, Programming and Computer Software, 2022, Vol. 48, No. 4, pp. 235–242. © Pleiades Publishing, Ltd., 2022.

One-class Classification for Identifying COVID-19 in X-Ray Images

Eduardo Perez-Careta[a,*], Delia Irazú Hernández-Farías[b,], José Rafael Guzman-Sepulveda[c,***], Miguel Torres Cisneros[a,****], Teodoro Cordoba-Fraga[b,*****], Juan Carlos Martinez Espinoza[c,******], and Rafael Guzman-Cabrera[a,d,*******]**

[a] *DICIS, Universidad de Guanajuato Campus Irapuato-Salamanca, Guanajuato, Gto., 36000 México*

[b] *DCI, Universidad de Guanajuato Campus León, León, Gto., 37150, México*

[c] *Centro de Investigación y de Estudios Avanzados del IPN, Unidad Monterrey, México*

[d] *Instituto Politécnico Nacional – UPIIG, Silao, Gto., 36275, México*

**e-mail: perez.e@ugto.mx*

***e-mail: di.hernandez@ugto.mx*

****e-mail: jose.guzmans@cinvestav.mx*

*****e-mail: mtorres@ugto.mx*

******e-mail: theo@fisica.ugto.mx*

*******e-mail: jcmartineze@ipn.mx*

********e-mail: guzmanc@ugto.mx*

Received January 29, 2021; revised November 20, 2021; accepted December 21, 2021

Abstract—Coronaviruses constitute an extensive family of viruses that can be severely harmful to both animals and humans. The newest virus of this family, SARS-CoV-2, and its associated disease in humans, COVID-19, have become a worldwide problem that requires bringing together different strategies to deal with it. The affectations of COVID-19 largely vary among individuals, ranging from a lack of symptoms to death. One of the fingerprints of COVID-19 is the damage caused to the respiratory system, which is often diagnosed based on a chest X-ray. In this work, we present an approach for classifying chest radiographs to identify the presence of COVID-19. Three different one-class based classifiers were implemented, and different image pre-processing techniques were applied to the radiographs to identify the combination of pre-processing/classifier that leads to the best results. For experimental purposes, we make use two datasets: one containing images from patients with COVID-19, and the second one with chest X-ray images corresponding to patients diagnosed with various acute respiratory conditions as well as healthy patients. The obtained results validate the feasibility of using the proposed methodology as an aid in the diagnosis of COVID-19.

Keywords: Diagnosis of Covid-19, one class classification, image classification

DOI: 10.1134/S0361768822040041

1. INTRODUCTION

At the end of 2019, the first case of the novel coronavirus disease, COVID-19, was detected. Some weeks later, it spreads around the world provoking a severe pandemic that has overwhelmed the health systems worldwide [1, 2]. Many efforts have been made to slow down the spread of the COVID-19. It has been recognized that being capable of delivering timely diagnostics is crucial to optimize the available resources at hospitals, health centers, and clinical facilities. In this regard, medical imaging based on X-ray and CT-scans has been one of the strategies used by the experts for detecting this disease [3, 4]. However, to correctly interpret these images, many radiologists are needed.

In such a situation, having automatic detection systems could help to save both time and human resources during the diagnostic phase [5, 6].

In recent years, the use of Artificial Intelligence (AI) in the medical field has shown an outstanding growth, and it has been successfully exploited for addressing different tasks, including the early-stage detection of diseases based on medical images [7]. A similar approach could also be applicable for the diagnosis of COVID-19. We have witnessed great contributions from computer sciences research projects, especially for the development of automatic diagnosis tools based on chest X-ray and chest CT-scans, which are encouraging and hold great hope for the early detection of COVID-19.

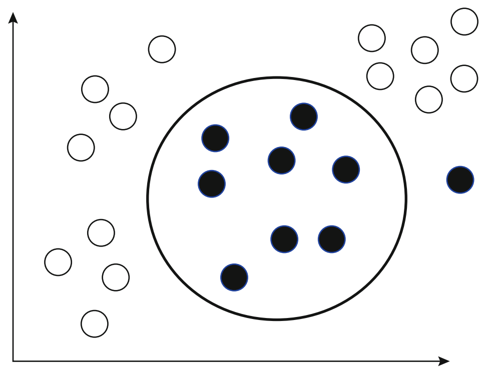

Fig. 1. Identification of samples of interest using an OCC.

In this sense, machine learning and image processing techniques are exploited to determine features that can serve to characterize this disease. Most of the research carried out for the automatic detection of COVID-19 based on medical images has been done by exploiting Deep Learning-based (hereafter DL-based) approaches. For instance, an approach for detecting COVID-19 in chest X-ray images using a Convolutional CapsNet has been proposed in [8]. It was evaluated in two different settings: a binary classification (COVID-19 and No-Findings), and multiclass classification (COVID-19, No-Findings, and Pneumonia). In [9], the authors proposed a DL approach where a hierarchical classification is carried out. In a first stage, the system determines if a chest X-ray is related to a healthy patient or to a patient with pulmonary disease; then, it discriminates between a generic pulmonary disease and COVID-19; and, finally, the method highlights the symptomatic areas in the X-ray. A Deep Convolutional Neural Network developed for object detection was also used for classifying chest X-ray from COVID-19 and pneumonia [5]. Furthermore, a Deep Convolutional Neural Network denoted as CoroNet was proposed in [10]. CoroNet is based on X-ception architecture pre-trained on ImageNet [10], it was evaluated on chest X-ray from COVID-19 and other chest pneumonia. A patch-based deep neural network with random patch cropping was proposed in [11]. COVNet [12] is a neural network developed for detecting COVID-19 by exploiting visual features from chest CT scans. Images of people suffering from community-acquired pneumonia as well as other related abnormalities were used together with CT scans of patients with COVID-19. Transfer learning has been also exploited for COVID-19 patients classification using CT scans [13].

An important drawback of the DL methodology is the need for a large amount of data required for training. Unfortunately, even with the increasing amount of daily diagnosis, nowadays there are only a few COVID-19 datasets available for researching purposes. In order to overcome this limitation, researchers have applied different techniques to increase the size of the database of the target class (COVID-19) such as data augmentation [14, 15] and transfer learning [13].

In this paper, we propose a different approach. Instead of attempting to compensate for the few data available, we propose using a different classification scheme that has not been explored before in this challenging task. We performed a one-class classification (OCC) based on an X-ray database that combines radiographs from patients that are healthy, and patients diagnosed with COVID-19 as well as several other pulmonary conditions. In OCC, the class boundary is defined by using the knowledge only from the class of interest [16], i.e., images from COVID-19 diagnosed patients, thus allowing to discriminate cases of patients with COVID-19 into one class and any other case (no-COVID-19) in the other. The OCC implements intelligent categorization of cases belonging to a specific class, among an existing set of records [16]. This type of binary classification has been used previously [8], and it is useful for cases where one is interested only in the membership to a specific target class. In our case, we are only interested in the binary classification of an X-ray image as "covid" or "no covid," while neglecting memberships to other classes e.g., pneumonia, SARS, or tuberculosis. We show that this approach can also be used to overcome the issues of data availability, and, at the same time, it discriminates COVID-19 images from other acute respiratory diseases.

The rest of the document is organized as follows. Section 2 introduces the OCC paradigm as well as the specific algorithms we used. Section 3 describes the proposed approach for classifying X-ray images. The experimental settings and results are presented in Section 4. Finally, the conclusions and future work are presented in Section 5.

2. ONE-CLASS CLASSIFICATION

Automatic classification is an important, engaging, and challenging research topic in image processing and pattern recognition, especially in medical applications for the automatic and early-stage diagnosis of diseases [11, 17, 18]. In this regard, classical OCC is meant to distinguish between normal and abnormal samples [19, 20]. Figure 1 shows a representation of an OCC, which separates the samples of interest (inside the circle) from the rest of the samples. In our case, the class of interest corresponds to the images that show the presence of COVID-19, which must be separated from the rest of the images. Carrying out this separation is not a trivial task, even for a human, because there is a need to identify characteristics that allow these images to be separated from the rest.

A widely used methodology for tackling binary classification problems is based on Support Vector Machines (SVM), with the aim of a single target class,

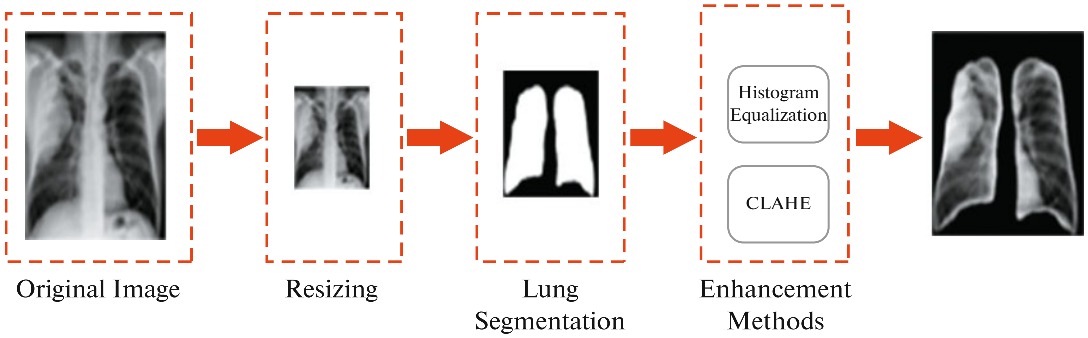

Fig. 2. Schematic representation of the preprocessing stage of RX images using our approach.

as first introduced by Vapnik [21]. Several variants of SVM have been proposed by researchers such as least-squares SVM; linear programming SVM; sparse SVM; twin SVM; Universum SVM; and, twin spheres SVM, among others [22–24]. Hybrid approaches combining SVM-based techniques with feature extractors have also been developed to compress the input data to lower dimensionalities [25–27].

Other OCC approaches use the reconstruction error of autoencoders [28] trained with only normal examples as an anomaly score [29–31]. In this task, the goal is to detect samples which are unseen by the training set. Self-representation learning and statistical modeling [32] are two widely used approaches for solving the OCC task. In [33], appearance and motion were proposed to extract features of video surveillance datasets. Based on the features learned, several OCC-SVM models were used to predict the anomaly scores and classify each frame as normal or anomalous. A similar procedure was presented in [34], where two approaches were used to learn regular motion patterns from video sequences. The most popular method that uses such an approach is based on variants of OCC-SVM [35]. Several approaches have been studied in [15, 36, 37] which use different OCC methods. Zhu et al. [14] have introduced the data and feature ensemble. In [38], the authors used one-class extreme learning machines (ELM) for liver tumor detection. Tax and Laskov [39] have developed an SVM-based OCC, for incremental and online learning. One-class Random Forest (OCRF) [40] is an appropriate choice for anomaly/novelty detection because it is flexible and does not suffer from the problem of overfitting. In [41], a cost-sensitive OCC-SVM algorithm for intrusion detection has been proposed. Their experiments have suggested that giving different cost or importance to system users than processes results in higher performance in intrusion detection.

On the other hand, in the case of isolation forest, the word "isolation" means separating an instance from the rest. This process is carried out, in most cases, in two stages: training and testing [42]. The training stage builds isolation trees using subsamples of the training set. The testing stage passes the test instances through isolation trees to obtain an anomaly score for each instance. This method of classifying instances has been widely used in the classification of medical images. The use of this method of classification in medical images is very widespread in the state of the art and ranges from skin lesions [43] to COVID-19 [44], as in our case.

3. OUR APPROACH

We used an OCC scheme to identify patients with COVID-19 based on chest X-ray. Two main stages can be identified in our approach: the image pre-processing stage and classification stage. The pre-processing stage is shown schematically in Fig. 2.

The preprocessing stage consists mainly of an image segmentation to isolate the lungs as the region of interest, as it has been suggested in the literature [18], followed by the contrast enhancement of the segmented chest X-ray based on standard methods. Then, we describe each step in more detail:

• ***Resizing and color standardization.*** The first step in the pre-processing stage consists of re-sizing the input image to dimensions of 512×512 pixels. In this step, we also built a color version of the resized image by replicating the grayscale layer into the RGB channels.

• ***Lung segmentation.*** To remove potential noise in the radiographs e.g., metadata and expert's annotations, we isolated the lungs regions. To this end, we used the model developed for lung segmentation in particularly, we used the "resnet34" model for generating the lungs' masks.

For training the network, the data provided in the same source was used. Attempting to minimize the noise in the resulting mask for the images, we applied the morphological operations of *erosion* and *dilation* to the binary mask before using it on the original chest X-rays. The operations implemented are: (a) *morphOpOne* for increasing the white regions in the edges of the obtained masks; (b) *morphOpTwo* for reducing the small white regions that are outside of the area of

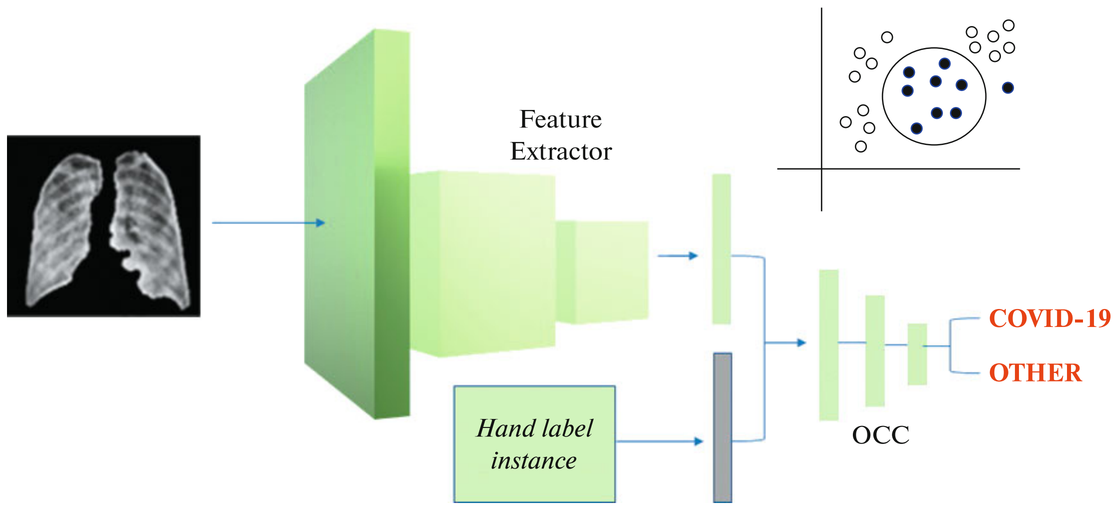

Fig. 3. Schematic representation of the one-class image classification stage in our approach.

interest; and (c) *morphOpThree* for removing the black holes inside the area of interest. In this part of the pre-processing, we exploited the aforementioned datasets for training the lung segmentation phase, afterwards these data have not been using during the feature extraction and classification stage.

Enhancement methods. The images are from different hospitals where the image acquisition was not performed under the same conditions or with the same equipment thus leading to variations in the image quality. To mitigate this, we used two widely applied image processing techniques, the *Histogram Equalization* (denoted as *HistEqu*) and the *Contrast Limited Adaptive Histogram Equalization* (denoted as *CLAHE*), to improve the contrast of the X-ray image. These routines are available in OpenCV Python [45].

In Fig. 3 we can see a schematic representation of the classification stage. A feature extraction module based on a widely recognized Convolutional Neural Network is used to generate a feature vector for each image. Then, an OCC algorithm is used to determine if a given chest X-ray belongs to a patient having COVID-19.

Feature extraction. After pre-processing, we used the well-known convolutional neutral network ResNet50 [18], which is pre-trained with ImageNet, to extract a feature vector from each image that was further used for feeding the classification algorithms. For doing so, each image was resized to 224 × 224 pixels to fit the requirements of the afore mentioned model. It is important to highlight that, in the feature extraction stage is the only one where we are using the pretrained CNN.

4. EXPERIMENTS AND RESULTS

4.1. Data

As mentioned before, datasets comprising medical images related to COVID-19 are scarce. This is due to the inherent challenges involving the development of a large set of manually annotated data, as it has been recognized [14, 46]. For experimental purposes, we worked with a dataset comprising two different corpora of chest X-ray. One of them, denoted as COVID-19 X-ray images[1] [46] includes different radiology images collected from hospitals in different countries. Nowadays, this is the most widely used dataset for investigating the COVID-19 from a ML perspective. The other one is the Montgomery County chest X-ray set[2] [47] that was developed for researching in the presence of Pulmonary Tuberculosis. It comprises chest X-Rays of both healthy people and those having some kinds of abnormalities. These datasets are briefly described below:

• The ***COVID-19 X-ray images*** comprises both chest X-ray and CT images from patients having COVID-19 or other viral and bacterial pneumonias. Besides the images, metadata are available. We used only the chest X-ray images. At the time we collected the data, there were cases where several images were available per patient; we used only one image per patient. We used a total of 153 images distributed as follows: *COVID-19*: 121 images; *COVID-19* and *ARDS*: 5 images; *Klebsiella*: 1 image; *Streptococcus*: 4 images; *ARDS*: 4 images; *Pneumocystis*: 7 images; *Legionella*: 2 images; *SARS*: 8 images; and *E. coli*: 1 image.

[1] It is publicly available in https://github.com/ieee8023/covid-chestxray-dataset

[2] It is publicly available in https://lhncbc.nlm.nih.gov/publication/pub9931

• The ***Montgomery County chest X-ray set*** dataset was collected in the framework of the control program of the Department of Health and Human Services of Montgomery County, Maryland, USA. It contains 138 posterior-anterior X-rays distributed in two classes: *80 normal* (i.e., healthy patients) and *58 abnormal* with manifestations of tuberculosis. The dataset covers a wide range of abnormalities such as effusions and miliary patterns. The images have a size around 4000 × 4000 pixels. Apart from the chest X-rays images, manual lung segmentations are available. It is important to highlight that both corpora we used have been used in the literature [5, 9, 11], but using different settings to the ones used here.

4.2. Experimental Settings and Results

As mentioned before, in our OCC approach chest X-ray images of confirmed cases of COVID-19 are the *target class* and all the other conditions (healthy, viral, and bacterial pneumonias, tuberculosis, etc.), constitute the OTHER class, i.e., the one with the majority number of instances. For evaluating the proposed approach, we included a total of ***126*** images labeled as *COVID-19* and ***165*** images belonging to the *OTHER* class. The classes are unbalanced on purpose to somewhat resemble a realistic scenario where a radiologist must be able to distinguish between different lung abnormalities, healthy, and people with COVID-19.

As mentioned before, we applied the methodology described in Section 3. In order to assess each of the steps included in our approach, we performed a set of experiments by combining the different processes mentioned:

(a) Experiments without enhancement:

i. Resizing

ii. Resizing + LungSegmentation

iii. Resizing + LungSegmentation + morphOpOne

iv. Resizing + LungSegmentation + morphOpTwo

v. Resizing + LungSegmentation + morphOpThree

(b) Experiments enhancement with *Histogram Equalization*:

i. Resizing + HistEqu

ii. Resizing + LungSegmentation + HistEqu

iii. Resizing + LungSegmentation + morphOpOne + HistEqu

iv. Resizing + LungSegmentation + morphOpTwo + HistEqu

v. Resizing + LungSegmentation + morphOpThree + HistEqu

(c) Experiments enhancement with *Contrast Limited Adaptive Histogram Equalization*

i. Resizing + CLAHE

ii. Resizing + LungSegmentation + CLAHE

iii. Resizing + LungSegmentation + morphOpOne + CLAHE

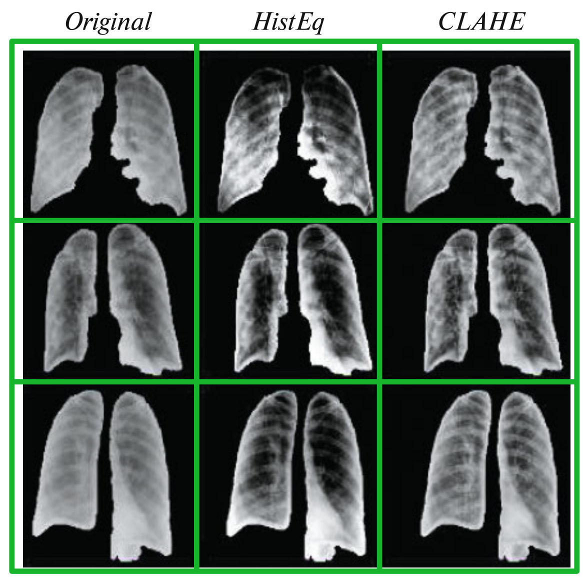

Fig. 4. Result of applying the mask and the enhancement methods to sample images.

iv. Resizing + LungSegmentation + morphOpTwo + CLAHE

v. Resizing + LungSegmentation + morphOpThree + CLAHE

Figure 4 shows some examples of the outcome after applying different processing. The first two rows belong to patients having a confirmed diagnostic of *COVID-19*. While the last one, represents an instance from the *OTHER* class. In the first column, the result of applying the corresponding mask to the *ORIGINAL* image is shown. While the remaining two are examples of the *HistEqu* and *CLAHE* enhancements methods. In all the samples, the respective mask was not modified by any morphological operation. As can be noticed, by applying the enhancement methods serves for in some way emphasize potential clues for distinguish between lungs from patients with COVID-19.

Classification Stage

For experimental purposes, we exploited the Scikit Learn[3] implementation of two OCC algorithms namely: OCC SVM (two different kernels were used: Linear and RBF), and OCC Isolated Forest. Besides, as baseline we decided to exploit a binary-based Dummy classifier[4]. Default parameters without any optimization were used for all classifiers. Tables 1, 2, and 3 show the obtained results. Specifically, we show the F-measure, see Eq. (1), for different classification schemes that were performed on X-ray images pre-processed in different ways.

[3] https://scikit-learn.org/stable/

[4] https://scikit-learn.org/stable/modules/generated/sklearn.dummy.DummyClassifier.html

Table 1. Obtained results in terms of F-measure for the experiments without enhancement

Pre-processing	RBF	Linear	Isolated forest	Dummy classifier
Resizing	0.54	0.42	**0.61**	0.45
Resizing + LungSegmentation	0.55	**0.57**	**0.61**	0.45
Resizing + LungSegmentation + morphOpOne	0.58	0.56	0.56	0.44
Resizing + LungSegmentation + morphOpTwo	**0.59**	0.54	0.56	0.46
Resizing + LungSegmentation + morphOpThree	0.56	0.48	0.58	0.46

Table 2. Obtained results in terms of F-measure for the experiments with Histogram Equalization

Pre-processing	RBF	Linear	Isolated forest	Dummy classifier
Resizing + HistEqu	**0.58**	0.44	0.60	0.46
Resizing + LungSegmentation + HistEqu	0.54	**0.53**	0.59	0.46
Resizing + LungSegmentation + morphOpOne + HistEqu	0.57	**0.53**	0.59	0.46
Resizing + LungSegmentation + morphOpTwo + HistEqu	0.56	0.48	**0.63**	0.45
Resizing + LungSegmentation + morphOpThree + HistEqu	0.54	0.45	0.58	0.47

$$F - measure = \frac{2 * Precision * Recall}{Precision + Recall}. \quad (1)$$

All the experiments were carried out under a five-fold cross validation setting, were for each fold the 70% of the instances were used for training and the remaining 30% for test that were selected randomly.

The best result was obtained by the OCC-SVM with the ***Isolated Forest*** with the pre-processing "Resizing + LungSegmentation + morphOpTwo + HistEqu." Most of the outcomes when the ***Linear*** kernel is used are around 0.5, except when using only "Resizing + LungSegmentation" processing where the result is 0.57. Regarding the ***RBF***, the best result, a 0.59 F-score, is obtained with the "Resizing + LungSegmentation." It is important to mention that, in all cases the obtained results outperform the baseline, even being built on a binary-classification scheme. Even when the obtained results are moderate, unlike other state-of-the-art models, particularly those using DL techniques, we are not using any data augmentation or oversampling technique, instead we are using a few but reliably images from patients with COVID-19.

5. CONCLUSIONS

In this work, we performed OCC of X-ray images from patients with COVID-19. We explored the impact of various pre-processing methods on the performance of the classifiers. More specifically, we used three classifiers of a single class on images that were pre-processed in fifteen different ways in order to determine which combination of pre-processing/classifier lead to the best results for the identification of the images of interest. We experimented with chest X-ray from patients having confirmed COVID-19 as the target class and in the OTHER class, the majority number of instances, images from a wide range of viral and bacterial types of pneumonia together with those from patients with Pulmonary Tuberculosis as well as some samples from healthy people. The classes are not balanced resembling in some way a realistic scenario where a radiologist must be able to distinguish between different lung abnormalities, healthy, and

Table 3. Obtained results in terms of F-measure for the experiments Contrast Limited Adaptive Histogram Equalization

Pre-processing	RBF	Linear	Isolated forest	Dummy classifier
Resizing + CLAHE	0.54	0.36	0.60	0.48
Resizing + LungSegmentation + CLAHE	**0.58**	0.51	**0.61**	0.45
Resizing + LungSegmentation + morphOpOne + CLAHE	0.57	0.52	0.57	0.45
Resizing + LungSegmentation + morphOpTwo + CLAHE	0.57	0.50	0.58	0.45
Resizing + LungSegmentation + morphOpThree + CLAHE	**0.58**	0.42	0.55	0.47

people with COVID-19. The best results considering the OCC-SVM approach are obtained with the Lung Segmentation and *morphOpOne* for increasing the white regions in the edges of the obtained masks. This process also has a favorable impact on the Isolated forest method, where it is also added and the contrast limited adaptive histogram equalization aiming to improve the contrast of the X-ray image. Finally, our approach is demonstrated to outperform a 'dummy', random classifier, and our results validate the use of the proposed approach.

CONFLICT OF INTEREST

The authors declare that they have no conflicts of interest.

REFERENCES

1. Mahase, E., China coronavirus: WHO declares international emergency as death toll exceeds 200, *Brit. Med. J.,* 2020, vol. 368, p. 408.
2. Cucinotta D. and Vanelli, M., WHO declares COVID-19 a pandemic, *Acta Biomed.: Atenei Parmensis,* 2020, vol. 91, pp. 157–160.
3. Zhang, J., Xie, Y., Li, Y., Shen, C., and Xia, Y., Covid-19 screening on chest x-ray images using deep learning based anomaly detection, 2020. arXiv:2003.12338
4. Xu, B., Xing, Y., Peng, J., Zheng, Z., Tang, W., Sun, Y., et al., Chest CT for detecting COVID-19: a systematic review and meta-analysis of diagnostic accuracy, *Eur. Radiol.,* 2020, vol. 30, no. 10, pp. 5720–5727.
5. Saiz, F.A. and Barandiaran, I., COVID-19 detection in chest X-ray images using a deep learning approach, *Int. J. Interact. Multimedia Artif. Intell.,* 2020, vol. 6, no. 2.
6. Ozturk, T., Talo, M., Yildirim, E.A., Baloglu, U.B., Yildirim, O., and Acharya, U.R., Automated detection of COVID-19 cases using deep neural networks with X-ray images, *Comput. Biol. Med.,* 2020, vol. 121, p. 103792.
7. Amisha, P.M., Pathania, M., and Rathaur, V.K., Overview of artificial intelligence in medicine, *J. Family med. Primary Care,* 2019, vol. 8, p. 2328.
8. Toraman, S., Alakuş, T.B., and Türkoğlu, İ., Convolutional CapsNet: a novel artificial neural network approach to detect COVID-19 disease from X-ray images using capsule networks, *Chaos, Solitons Fractals,* 2020, vol. 140, p. 110122.
9. Brunese, L., Mercaldo, F., Reginelli, A., and Santone, A., Explainable deep learning for pulmonary disease and coronavirus COVID -19 detection from X-rays, *Comput. Methods Programs Biomed.,* 2020, vol. 196, no. 20, p. 105608.
10. Khan, A.I., Shah, J.L., and Bhat, M.M., CoroNet: a deep neural network for detection and diagnosis of COVID-19 from chest X-ray images, *Comput. Methods Programs Biomed.,* 2020, vol. 196, no. 18, p. 105581.
11. Oh, Y., Park, S., and Ye, J.C., Deep learning COVID -19 features on cxr using limited training data sets, *IEEE Trans. Med. Imag.,* 2020, vol. 39, no. 8.
12. Li, L., Qin, L., Xu, Z., Yin, Y., Wang, X., Kong, B., et al., Artificial intelligence distinguishes COVID-19 from community acquired pneumonia on chest CT, *Radiology,* 2020, vol. 296, no. 2, p. 200905.
13. Jaiswal, A., Gianchandani, N., Singh, D., Kumar, V., and Kaur, M., Classification of the COVID-19 infected patients using DenseNet201 based deep transfer learning, *J. Biomol. Struct. Dyn.,* 2020, vol. 39, no. 1, pp. 1–8.
14. Zhu, W., Huang, W., Lin, Z., Yang, Y., Huang, S., and Zhou, J., Data and feature mixed ensemble based extreme learning machine for medical object detection and segmentation, *Multimedia Tools Appl.,* 2016, vol. 75, pp. 2815–2837.
15. Mũnoz-Marí, J., Bovolo, F., Gómez-Chova, L., Bruzzone, L., and Camp-Valls, G., Semisupervised one-class support vector machines for classification of remote sensing data, *IEEE Trans. Geosci. Remote Sens.,* 2010, vol. 48, pp. 3188–3197.
16. Khan, S.S. and Madden, M.G., One-class classification: taxonomy of study and review of techniques, *Knowl. Eng. Rev.,* 2014, vol. 29, pp. 345–374.
17. Sali, R., Ehsan, L., Kowsari, K., Khan, M., Moskaluk, C.A., Syed, S., et al., Celiacnet: celiac disease severity diagnosis on duodenal histopathological images using deep residual networks, in *Proc. IEEE Int. Conf. on Bioinformatics and Biomedicine (BIBM),* San Diego, CA, 2019, pp. 962–967.
18. Morales Castro, W. and Guzman Cabrera, R., Tuberculosis: diagnosis by image processing, *Comput. Sist.,* 2020, vol. 24, no. 2.
19. Schölkopf, B., Platt, J.C., Shawe-Taylor, J., Smola, A.J., and Williamson, R.C., Estimating the support of a high-dimensional distribution, *Neural Comput.,* 2001, vol. **13**, pp. 1443–1471.
20. Tax, D.M. and Duin, R.P., Support vector data description, *Mach. Learn.,* 2004, vol. 54, pp. 45–66.
21. Vapnik, V., *Statistical Learning Theory,* New York: Wiley-Intersci., 1998.
22. Tomar, D. and Agarwal, S., Twin support vector machine: a review from 2007 to 2014, *Egypt. Inf. J.,* 2015, vol. 16, pp. 55–69.
23. Zhao, J., Xu, Y., and Fujita, H., An improved non-parallel universum support vector machine and its safe sample screening rule, *Knowl.-Based Syst.,* 2019, vol. 170, pp. 79–88.
24. Lu, S., Wang, H., and Zhou, Z., All-in-one multicategory ramp loss maximum margin of twin spheres support vector machine, *Appl. Intell.,* 2019, vol. 49, pp. 2301–2314.
25. Xu, D., Ricci, E., Yan, Y., Song, J., and Sebe, N., Learning deep representations of appearance and motion for anomalous event detection, *Proc. British Machine Vision Conf.,* Swansea, 2015, pp. 8.1-8.12. arXiv:1510.01553
26. Erfani, S.M., Rajasegarar, S., Karunasekera, S., and Leckie, C., High-dimensional and large-scale anomaly detection using a linear one-class SVM with deep learning, *Pattern Recogn.,* 2016, vol. 58, pp. 121–134.
27. Andrews, J., Tanay, T., Morton, E.J., and Griffin, L.D., Transfer representation-learning for anomaly detection, *Proc. Anomaly Detection Workshop; Int. Conf. on Machine Learning, ICML 2016,* New York, 2016.

28. Hinton, G.E. and Salakhutdinov, R.R., Reducing the dimensionality of data with neural networks, *Science,* 2006, vol. 313, pp. 504–507.
29. Hawkins, S., He, H., Williams, G., and Baxter, R., Outlier detection using replicator neural networks, *Proc. Int. Conf. on Data Warehousing and Knowledge Discovery,* Aix-en-Provence, 2002, pp. 170–180.
30. An, J. and Cho, S., Variational autoencoder based anomaly detection using reconstruction probability, *Spec. Lect. IE,* 2015, vol. 2, pp. 1–18.
31. Chen, J., Sathe, S., Aggarwal, C., and Turaga, D., Outlier detection with autoencoder ensembles, *Proc. SIAM Int. Conf. on Data Mining,* Houston, 2017, pp. 90–98.
32. Xia, Y., Cao, X., Wen, F., Hua, G., and Sun, J., Learning discriminative reconstructions for unsupervised outlier removal, *Proc. IEEE Int. Conf. on Computer Vision,* Santiago, 2015, pp. 1511–1519.
33. Xu, D., Yan, Y., Ricci, E., and Sebe, N., Detecting anomalous events in videos by learning deep representations of appearance and motion, *Comput. Vision Image Understand.,* 2017, vol. 156, pp. 117–127.
34. Hasan, M., Choi, J., Neumann, J., Roy-Chowdhury, A.K., and Davis, L.S., Learning temporal regularity in video sequences, *Proc. IEEE Conf. on Computer Vision and Pattern Recognition,* Las Vegas, 2016, pp. 733–742.
35. Tax, D.M.J., One-class classification: concept learning in the absence of counter-examples, *Thesis,* Technische Universiteit Delft, 2002.
36. Wilk, T. and Wozniak, M., Soft computing methods applied to combination of one-class classifiers, *Neurocomputing,* 2012, vol. 75, pp. 185–193.
37. Roth, V., Kernel fisher discriminants for outlier detection, *Neural Comput.,* 2006, vol. 18, pp. 942–960.
38. Huang, W., Li, N., Lin, Z., Huang, G.-B., Zong, W., Zhou, J., et al., Liver tumor detection and segmentation using kernel-based extreme learning machine, *Proc. 35th Annu. IEEE Int. Conf. on Engineering in Medicine and Biology Society (EMBC),* Osaka, 2013, pp. 3662–3665.
39. Tax, D.M. and Laskov, P., Online SVM learning: from classification to data description and back, *Proc. 13th IEEE Workshop on Neural Networks for Signal Processing,* Toulouse, 2003, pp. 499–508.
40. Désir, C., Bernard, S., Petitjean, C., and Heutte, L., One class random forests, *Pattern Recogn.,* 2013, vol. 46, pp. 3490–3506.
41. Luo, J., Ding, L., Pan, Z., Ni, G., and Hu, G., Research on cost-sensitive learning in one-class anomaly detection algorithms, *Proc. Int. Conf. on Autonomic and Trusted Computing,* Hong Kong, 2007, pp. 259–268.
42. Liu, F.T., Ting, K.M., and Zhou, Z.-H., Isolation forest, *Proc. 8th IEEE Int. Conf. on Data Mining*, Pisa, 2008, pp. 413–422.
43. Li, X., Lu, Y., Desrosiers, C., and Liu, X., Out-of-distribution detection for skin lesion images with deep isolation forest, 2020. arXiv:2003.09365
44. Alafif, T., Alotaibi, R., Albassam, A., and Almudhayyani, A., On the prediction of isolation, release, and decease for COVID-19 patients: a case study in South Korea, *ISA Trans.,* 2022, vol. 124, pp. 191–196.
45. Bradski, G., The opencv library, *Dr Dobb's J. Software Tools,* 2000, vol. 25, pp. 120–125.
46. Cohen, J.P., Morrison, P., Dao, L., Roth, K., Duong, T.Q., and Ghassemi, M., Covid-19 image data collection: prospective predictions are the future, 2020. arXiv:2006.11988
47. Jaeger, S., Candemir, S., Antani, S., Wáng, Y.-X.J., Lu, P.-X., and Thoma, G., Two public chest X-ray datasets for computer-aided screening of pulmonary diseases, *Quant. Imag. Med. Surg.,* 2014, vol. 4, p. 475.